

# Study of the projected sensitivity on the anomalous quartic gauge couplings via $Z\gamma\gamma$ production at the CLIC

E. Gurkanli\*,<sup>1</sup> V. Ari†,<sup>2</sup> M. Köksal‡,<sup>3</sup> A. Gutiérrez-Rodríguez§,<sup>4</sup> and M. A. Hernández-Ruíz¶<sup>5</sup>

<sup>1</sup>*Department of Physics, Sinop University, Turkey.*

<sup>2</sup>*Department of Physics, Ankara University, Turkey.*

<sup>3</sup>*Department of Physics, Sivas Cumhuriyet University, 58140, Sivas, Turkey.*

<sup>4</sup>*Facultad de Física, Universidad Autónoma de Zacatecas  
Apartado Postal C-580, 98060 Zacatecas, México.*

<sup>5</sup>*Unidad Académica de Ciencias Químicas, Universidad Autónoma de Zacatecas  
Apartado Postal C-585, 98060 Zacatecas, México.*

(Dated: December 9, 2021)

arXiv:2112.03948v1 [hep-ph] 7 Dec 2021

---

\* egurkanli@sinop.edu.tr

† vari@science.ankara.edu.tr

‡ mkoksal@cumhuriyet.edu.tr

§ alexgu@fisica.uaz.edu.mx

¶ mahernan@uaz.edu.mx

## Abstract

Gauge boson self-couplings are completely defined by the non-abelian gauge symmetry of the Standard Model (SM), thus direct search for these couplings are extremely significant in understanding the gauge structure of the SM. However, the possible deviation from the SM predictions of gauge boson self-couplings would be a sign of the presence of new physics beyond the SM. In this work, we study the sensitivities on the anomalous couplings defined by dimension-8 operators related to the  $ZZ\gamma\gamma$  and  $Z\gamma\gamma\gamma$  quartic vertices through the process  $e^+e^- \rightarrow Z\gamma\gamma$  with Z-boson decaying to charged leptons at the Compact Linear Collider (CLIC). We analyze the center-of-mass energy of 3 TeV, integrated luminosities of  $\mathcal{L} = 1, 4, 5 \text{ ab}^{-1}$ , systematic uncertainties of  $\delta_{sys} = 0\%, 5\%, 10\%$ , and unpolarized and polarized electron beams for extraction of expected sensitivity on the anomalous  $f_{T,j}/\Lambda^4$  couplings at 95% confidence level, which are especially sensitive to the  $Z\gamma\gamma$  channel. It is clear from the results that if the systematic error is improved, we expect better limits on the couplings. However, the best limits obtained on the anomalous quartic couplings for the process  $e^+e^- \rightarrow Z\gamma\gamma$  with  $\sqrt{s} = 3 \text{ TeV}$ ,  $\mathcal{L} = 5 \text{ ab}^{-1}$  and  $\delta_{sys} = 0\%$  can be approximately improved up to about two times better than the limits obtained with  $\delta_{sys} = 10\%$ . Our sensitivities on the anomalous quartic couplings with  $\delta_{sys} = 0\%$  can set more stringent sensitivity by two orders of magnitude with respect to the best sensitivity derived from the current experimental limits. Finally, with initial electron beam polarization, the sensitivity of anomalous quadratic couplings improves by almost a factor of 1.2.

PACS numbers: 12.60.-i, 14.70.Hp, 14.70.Bh

Keywords: Electroweak interaction, Models beyond the Standard Model, Anomalous couplings.

## I. INTRODUCTION

In the Standard Model (SM) of the elementary particle physics, the structure of the fermion-vector boson couplings has been extensively tested [1–4]. However, other sectors of the SM, as the one corresponding for the self-couplings of the vector bosons, such as triple  $VVV$  and quartic  $VVVV$  couplings with  $V = \gamma, Z, W^\pm, H$  have been less tested. In this regard, the determination of these interactions can confirm the non-Abelian gauge structure of the theory and the mechanism of the spontaneous breaking of the electroweak symmetry. In addition, the study of the neutral gauge boson self-couplings provides one of the most sensitive probes of new physics beyond the SM (BSM) [4].

The physics program of the ATLAS and CMS Collaborations at the CERN Large Hadron Collider (LHC) contemplates the study of the physics of the anomalous Quartic Gauge Couplings (aQGC) and the anomalous Triple Gauge Couplings (aTGC), which are deviations from the SM [5–8]. In addition, scrutinize the study of the physics of the Higgs boson, top quark, tau lepton and dark matter. As triboson production and vector boson scattering (VBS) are directly sensitive to aQGC a detailed investigation might give deeper insights into the electroweak sector of SM and lead to the discovery of new physics. Current analyses do not have enough data at their disposal, but the upgrade of the ATLAS and CMS detector and future LHC runs with high luminosity will increase the sensitivity in the important regions. In the following, some studies on future results at the ATLAS experiment on QGC are presented. The L3 and OPAL Collaborations at the CERN LEP-II reported for the first time bounds on the aQGC  $ZZ\gamma\gamma$  coupling via  $e^+e^-$  collisions [9, 10]. Other studies are realized in hadron-hadron colliders by the D0 and CDF Collaborations at the Tevatron at Fermilab [11, 12] and by the ATLAS [13–17] and CMS Collaborations [18–28] at the LHC. Other processes and potential mechanisms for the phenomenological analyses of anomalous quartic neutral interactions are the followings,  $e^+e^- \rightarrow Z\gamma\gamma$  [29, 30],  $e^+e^- \rightarrow ZZ\gamma$  [31],  $e^+e^- \rightarrow qq\gamma\gamma$  [32],  $e^- \gamma \rightarrow ZZ e^-$  [33],  $e^- \gamma \rightarrow Z\gamma e^-$  [34],  $\gamma\gamma \rightarrow ZZ$  [35],  $e^+e^- \rightarrow ZZ\gamma$  [36],  $p\bar{p} \rightarrow Z\gamma\gamma$  [37],  $pp(\bar{p}) \rightarrow \gamma\gamma ll$  [38],  $pp \rightarrow p\gamma^*\gamma^*p \rightarrow pZZp$  [39–41],  $pp \rightarrow p\gamma^*p \rightarrow PZZqX$  [42],  $pp \rightarrow p\gamma^*p \rightarrow p\gamma ZqX$  [43],  $pp \rightarrow qq\gamma ll$  [44],  $pp \rightarrow Z\gamma\gamma$  [45].

It is appropriate to mention that the ATLAS and CMS Collaborations recently observed the  $pp \rightarrow Z\gamma\gamma \rightarrow l^+l^-\gamma\gamma$  production channel with center-of-mass energy of 8 TeV and integrated luminosity of  $20.3 \text{ fb}^{-1}$ , respectively [6, 7]. More recently, the first measure-

ments of the  $pp \rightarrow Z\gamma\gamma \rightarrow l^+l^-\gamma\gamma$  cross-section at  $\sqrt{s} = 13$  TeV is reported by the CMS Collaboration, corresponding to an integrated luminosity of  $\mathcal{L} = 137 \text{ fb}^{-1}$  [8].

Due to the nature of the colliding particles, lepton colliders are generally useful to examine the processes. Because the elementary particles are fully defined at the fundamental level, the collisions in lepton collider are clean without any hadronic activity, and the measurements are made more precisely. The hadron colliders have higher collision energies than lepton colliders. However, high collision energies play a crucial role in investigating the new particles and their interactions. On the other hand, each collision in hadron collider composes several backgrounds for physics analysis, creating a large number of elementary processes. Therefore, in hadron colliders, it is not easy to perform analysis and make precise measurements. The discovery potential of the LHC would be complemented by the CLIC, which is a multi-TeV high-luminosity linear  $e^+e^-$  collider under development.

The current CLIC baseline staging scenario assumes  $1.0 \text{ ab}^{-1}$ ,  $2.5 \text{ ab}^{-1}$  and  $5.0 \text{ ab}^{-1}$  of luminosity at the three energy stages of  $\sqrt{s} = 0.38$  TeV, 1.5 TeV and 3 TeV, respectively[46]. Also, the baseline CLIC provides  $\pm 80\%$  longitudinal polarisation for the electron beam and no positron polarisation. The expected integrated luminosities for the CLIC with the polarized electron beams are  $\mathcal{L} = 1 \text{ ab}^{-1}$  ( $P_{e^-} = 80\%$ ),  $\mathcal{L} = 4 \text{ ab}^{-1}$  ( $P_{e^-} = -80\%$ ) and  $\mathcal{L} = 5 \text{ ab}^{-1}$  ( $P_{e^-} = 0\%$ ) [46]. Thanks to the clean event environment, the tunable collision energy and the potential to polarize beams, it is possible for the CLIC that observe the deviation from SM predictions indicating new physics, discover new particles and make precise measurements. Furthermore, beam polarisations combined with high luminosity increase the analysis capability, resulting in better statistics, reducing systematic errors, enhancing the signal or suppressing the SM processes, and revealing new processes. Thus, the use of polarized electron beams is beneficial in increasing signal rates and minimizing unwanted background processes.

The cross-section of any process is defined from the four possible pure chiral cross-sections with electron beam polarizations  $P_{e^-}$  and positron beam polarization  $P_{e^+}$  as follows [47]

$$\begin{aligned} \sigma(P_{e^-}, P_{e^+}) = \frac{1}{4} \{ & (1 + P_{e^-})(1 + P_{e^+})\sigma_{RR} + (1 - P_{e^-})(1 - P_{e^+})\sigma_{LL} \\ & + (1 + P_{e^-})(1 - P_{e^+})\sigma_{RL} + (1 - P_{e^-})(1 + P_{e^+})\sigma_{LR} \}, \end{aligned} \quad (1)$$

where  $\sigma_{RR}$  and  $\sigma_{LL}$  represent the cross-sections of both right-handed electron and positron

beams and both left-handed electron and positron beams, respectively. On the other hand,  $\sigma_{LR}$  and  $\sigma_{RL}$  show the cross-sections of left-handed electron and right-handed positron beams and vice versa. The unpolarized cross-section  $\sigma_0$  can be given as

$$\sigma_0 = \frac{1}{4} \{ \sigma_{RR} + \sigma_{LL} + \sigma_{RL} + \sigma_{LR} \}. \quad (2)$$

In this paper, the process  $e^+e^- \rightarrow Z\gamma\gamma \rightarrow l^+l^-\gamma\gamma$  at the CLIC with unpolarized and polarized electron beams are used to investigate the presence of new physics parametrized as the aQGC between the Z boson and the photons. Here, the systematic uncertainties are included in the analysis. In the final state, electron and muon channels are combined to get better sensitivity on the aQGC parameters. The paper is organized as follows. In Section II, we give a brief description of the dimension-8 effective field theory approach for the aQGC  $ZZ\gamma\gamma$  and  $Z\gamma\gamma\gamma$ . The study of the  $Z\gamma\gamma$  signal, as well as the sensitivity on the  $f_{T,j}/\Lambda^4$  couplings at 95% confidence level (C.L.) at the CLIC are discussed in Section III. Finally, we summarize our conclusions in Section IV.

## II. DIMENSION-8 EFFECTIVE OPERATORS FOR THE $Z\gamma\gamma$ AND $ZZ\gamma\gamma$ AQGC

With the discovery of the Higgs boson, and the measurements of its properties at the LHC, the general features of the SM electroweak theory have been confirmed experimentally [48]. Measurements of the Higgs couplings and production rates agree with SM predictions and there is no indication of the existence of any new particle at the TeV scale [4]. Going forward, the task is to make comparisons between theory and data at the few percent levels. This requires not only high-luminosity LHC running, but also improved theoretical calculations.

$Z\gamma\gamma$  triple production is an example of a process whose properties are restricted by LEP-II measurements [9, 10], yet still provides relevant information about the  $Z\gamma\gamma\gamma$  and  $ZZ\gamma\gamma$  couplings from LHC data. The production of  $Z\gamma\gamma$  triple provides a sensitive test of the electroweak gauge structure of the SM and check for non-SM aQGC.

BSM physics effects in  $Z\gamma\gamma$  production can be studied using effective Lagrangian techniques where the new physics is parameterized as an operator expansion in inverse powers of a high scale,  $\Lambda$ . In this regard, the extension of the effective SM-Lagrangian is done by introducing additional dimension-8 operators for the aQGC. The formalism of the aQGC

has been widely discussed in the literature [49–55]. The effective Lagrangian that gives all quartic couplings is given as follows

$$\mathcal{L}_{eff} = \mathcal{L}_{SM} + \sum_{k=0}^1 \frac{f_{S,k}}{\Lambda^4} O_{S,k} + \sum_{i=0}^7 \frac{f_{M,i}}{\Lambda^4} O_{M,i} + \sum_{j=0,1,2,5,6,7,8,9} \frac{f_{T,j}}{\Lambda^4} O_{T,j}, \quad (3)$$

where each  $O_{S,k}$ ,  $O_{M,i}$  and  $O_{T,j}$  is a gauge-invariant operator of dimension-8 and  $\frac{f_{S,k}}{\Lambda^4}$ ,  $\frac{f_{M,i}}{\Lambda^4}$  and  $\frac{f_{T,j}}{\Lambda^4}$  are the corresponding effective coefficient. According to the structure of the operator, there are three classes of genuine aQGC operators as shown in Eq. (3) [53, 55].

The dimension-8 operators given by Eq. (3) contains contributions of Higgs boson field ( $\frac{f_{S,k}}{\Lambda^4} O_{S,k}$ ), Higgs-Gauge boson field ( $\frac{f_{M,i}}{\Lambda^4} O_{M,i}$ ) and Gauge boson field ( $\frac{f_{T,j}}{\Lambda^4} O_{T,j}$ ), corresponding to the occurrence of the building blocks above. The corresponding genuine aQGC operators of these contributions are presented below.

- Contribution of operators with covariant derivatives only (Scalar field):

$$O_{S,0} = [(D_\mu \Phi)^\dagger (D_\nu \Phi)] \times [(D^\mu \Phi)^\dagger (D^\nu \Phi)], \quad (4)$$

$$O_{S,1} = [(D_\mu \Phi)^\dagger (D^\mu \Phi)] \times [(D_\nu \Phi)^\dagger (D^\nu \Phi)]. \quad (5)$$

- Contribution of operators with Gauge boson field strength tensors only (Tensor field):

$$O_{T,0} = Tr[W_{\mu\nu} W^{\mu\nu}] \times Tr[W_{\alpha\beta} W^{\alpha\beta}], \quad (6)$$

$$O_{T,1} = Tr[W_{\alpha\nu} W^{\mu\beta}] \times Tr[W_{\mu\beta} W^{\alpha\nu}], \quad (7)$$

$$O_{T,2} = Tr[W_{\alpha\mu} W^{\mu\beta}] \times Tr[W_{\beta\nu} W^{\nu\alpha}], \quad (8)$$

$$O_{T,5} = Tr[W_{\mu\nu} W^{\mu\nu}] \times B_{\alpha\beta} B^{\alpha\beta}, \quad (9)$$

$$O_{T,6} = Tr[W_{\alpha\nu} W^{\mu\beta}] \times B_{\mu\beta} B^{\alpha\nu}, \quad (10)$$

$$O_{T,7} = Tr[W_{\alpha\mu} W^{\mu\beta}] \times B_{\beta\nu} B^{\nu\alpha}, \quad (11)$$

$$O_{T,8} = B_{\mu\nu} B^{\mu\nu} B_{\alpha\beta} B^{\alpha\beta}, \quad (12)$$

$$O_{T,9} = B_{\alpha\mu} B^{\mu\beta} B_{\beta\nu} B^{\nu\alpha}. \quad (13)$$

- Contribution of both operators with covariant derivatives and field strength tensors (Mixed field):

$$O_{M,0} = Tr[W_{\mu\nu}W^{\mu\nu}] \times [(D_\beta\Phi)^\dagger(D^\beta\Phi)], \quad (14)$$

$$O_{M,1} = Tr[W_{\mu\nu}W^{\nu\beta}] \times [(D_\beta\Phi)^\dagger(D^\mu\Phi)], \quad (15)$$

$$O_{M,2} = [B_{\mu\nu}B^{\mu\nu}] \times [(D_\beta\Phi)^\dagger(D^\beta\Phi)], \quad (16)$$

$$O_{M,3} = [B_{\mu\nu}B^{\nu\beta}] \times [(D_\beta\Phi)^\dagger(D^\mu\Phi)], \quad (17)$$

$$O_{M,4} = [(D_\mu\Phi)^\dagger W_{\beta\nu}(D^\mu\Phi)] \times B^{\beta\nu}, \quad (18)$$

$$O_{M,5} = [(D_\mu\Phi)^\dagger W_{\beta\nu}(D^\nu\Phi)] \times B^{\beta\mu}, \quad (19)$$

$$O_{M,6} = [(D_\mu\Phi)^\dagger W_{\beta\nu}W^{\beta\nu}(D^\mu\Phi)], \quad (20)$$

$$O_{M,7} = [(D_\mu\Phi)^\dagger W_{\beta\nu}W^{\beta\mu}(D^\nu\Phi)]. \quad (21)$$

In the set of genuine aQGC operators given in Eqs. (4)-(21),  $\Phi$  stands for the Higgs doublet, and the covariant derivatives of the Higgs field is given by  $D_\mu\Phi = (\partial_\mu + igW_\mu^j\frac{\sigma^j}{2} + \frac{i}{2}g'B_\mu)\Phi$ , and  $\sigma^j$  ( $j = 1, 2, 3$ ) represent the Pauli matrices, while  $W^{\mu\nu}$  and  $B^{\mu\nu}$  are the gauge field strength tensors for  $SU(2)_L$  and  $U(1)_Y$ .

In Table I, a list of all the genuine aQGC modified by dimension-8 operators are presented. In particular, the  $Z\gamma\gamma$  channel is especially sensitive to the  $f_{T,0}/\Lambda^4$ ,  $f_{T,1}/\Lambda^4$ ,  $f_{T,2}/\Lambda^4$ ,  $f_{T,5}/\Lambda^4$ ,  $f_{T,6}/\Lambda^4$ ,  $f_{T,7}/\Lambda^4$ ,  $f_{T,8}/\Lambda^4$ , and  $f_{T,9}/\Lambda^4$  operators. For this reason, we consider only these operators in our study. However, limits obtained for the  $f_{T,8}/\Lambda^4$  and  $f_{T,9}/\Lambda^4$  coupling parameters are of interest because they can be extracted only by studying the production of Electroweak neutral bosons.

It is important to note that the operators in Eq. (3) lead to tree-level unitarity violation. This is because the effective field theory is not a complete model and violates unitarity at sufficiently high energy scales. However, the standard procedure to avoid this unphysical behavior of the cross-section and to obtain meaningful limits is to multiply the anomalous couplings by a form factor of the form [52]:

$$FF = \frac{1}{(1 + \frac{\hat{s}}{\Lambda_{FF}^2})^2} \quad (22)$$

In Eq. (22),  $\hat{s}$  corresponds to the squared invariant mass of the produced bosons and  $\Lambda_{FF}$  is the energy scale of the form factor, which corresponds to the energy regime above which the contributions of the anomalous couplings are largely suppressed. For triboson processes there is no theoretical algorithm to compute the appropriate value for to avoid unitarity violation.

TABLE I: The aQGC altered with dimension-8 operators are shown with X.

	WWWW	WWZZ	ZZZZ	WW $\gamma$ Z	WW $\gamma\gamma$	ZZZ $\gamma$	ZZ $\gamma\gamma$	Z $\gamma\gamma\gamma$	$\gamma\gamma\gamma\gamma$
$O_{S0}, O_{S1}$	X	X	X						
$O_{M0}, O_{M1}, O_{M6}, O_{M7}$	X	X	X	X	X	X	X		
$O_{M2}, O_{M3}, O_{M4}, O_{M5}$		X	X	X	X	X	X		
$O_{T0}, O_{T1}, O_{T2}$	X	X	X	X	X	X	X	X	X
$O_{T5}, O_{T6}, O_{T7}$		X	X	X	X	X	X	X	X
$O_{T8}, O_{T9}$			X			X	X	X	X

Therefore, the confidence intervals in this analysis are derived using three different values of 0.5, 1 TeV and  $\infty$  [16]. The latter corresponds to the non-unitarised case, which is evaluated to allow for the comparison with other analyses.

### III. ELECTROWEAK $Z\gamma\gamma$ PRODUCTION AT THE CLIC AND SENSITIVITY ON AQGC

#### A. Sensitivity of cross-section of the $e^+e^- \rightarrow Z\gamma\gamma$ signal

The total cross-section of the process  $e^+e^- \rightarrow Z\gamma\gamma \rightarrow l^+l^-\gamma\gamma$  where  $Z$  boson subsequently decays to  $e^+e^-$  or  $\mu^+\mu^-$  pairs, receives contributions from five Feynman diagrams at the tree-level as shown in Fig. 1. The first two diagrams give the anomalous contribution for  $Z\gamma\gamma\gamma$  and  $ZZ\gamma\gamma$  vertices, while the remaining diagrams give the contribution of the SM backgrounds.

The signal involves nonzero the aQGC and the SM contribution as well as its interference. Here, SM represents the SM background process of the same final state with the signal in our analyse. Also, we consider that there are also other backgrounds such as  $e^-e^+ \rightarrow \tau\tau\gamma\gamma$  and  $e^-e^+ \rightarrow \gamma\gamma\gamma\ell\ell$ . Therefore, in this work, we study the features of the total cross-section  $\sigma\left(\sqrt{s}, \frac{f_{T,j}}{\Lambda^4}\right)$ , the number of events of the signals, SM and relevant backgrounds processes, as well as the sensitivity on the anomalous  $f_{T,j}/\Lambda^4$  couplings using the MadGraph5\_aMC@NLO [56] toolkit, where the operators are given in Eqs. (6) and (13) are implemented into

TABLE II: Particle-level selections cuts for the  $Z\gamma\gamma$  signal at the CLIC.

Kinematic cuts	$f_{Tj}/\Lambda^4$
Cut-1	$p_T^l > 25 \text{ GeV} ,  \eta^l  < 2.5$
Cut-2	$ \eta^\gamma  < 2.5$
Cut-3	$\Delta R(\gamma_1, \gamma_2) > 0.4 , \Delta R(\ell_1, \ell_2) > 0.4 , \Delta R(\gamma_1, \ell_2) > 0.4$
Cut-4	$80 \text{ GeV} < M_{\ell+\ell^-} < 100 \text{ GeV}$
Cut-5	$p_T^\gamma > 300 \text{ GeV}$

MadGraph5\_aMC@NLO through Feynrules package [57] as a Universal FeynRules Output (UFO) module [58].

We apply the kinematic selection cuts to suppress the backgrounds and to optimize the signal sensitivity.  $p_T^l, p_T^\gamma$  are the transverse momenta of the final state leptons and the photons,  $\eta^l$  and  $\eta^\gamma$  are the pseudorapidities of the leptons and the photons. Here, we consider  $p_T^l > 25 \text{ GeV}$  and  $\eta^l < 2.5$  with tagged Cut-1,  $\eta^\gamma < 2.5$  with tagged Cut-2. To have well-separated photons and charged leptons in the phase space, we require angular separations ( $\Delta R = ((\Delta\phi)^2 + (\Delta\eta)^2)^{1/2}$ ) between charged lepton and photon in the pseudorapidity-azimuthal angle plane that are  $\Delta R(\gamma_1, \gamma_2) > 0.4 , \Delta R(l_1, l_2) > 0.4 , \Delta R(\gamma_1, l_2) > 0.4$  with tagged Cut-3. The pairing ambiguity is resolved by ordering the pair of dilepton candidates based on the differences between the reconstructed invariant mass of the dilepton candidate and the nominal  $Z$  boson mass  $m_Z$ . Therefore, the dilepton candidate with an invariant mass closest to the nominal  $Z$  boson mass is applied  $80 < M_{l+l^-} < 100 \text{ GeV}$  with tagged Cut-4. Production of  $Z\gamma\gamma$  events with photons with large transverse momentum  $p_T^\gamma$  is a sensitive probe of physics BSM. This final stage has the advantage of being identifiable with high efficiency and purity. In this sense, it is known that the high dimensional operators could affect  $p_T^\gamma$  photon transverse momentum, especially at the region with large  $p_T^\gamma$  values, which is very useful to distinguish between signal and background events. Since requiring the high transverse momentum photon eliminates the fake backgrounds, the numbers of expected events as a function of  $p_T^\gamma$  photon transverse momentum for the  $e^+e^- \rightarrow Z\gamma\gamma$  signal and backgrounds at the CLIC with  $\sqrt{s} = 3 \text{ TeV}$ ,  $P_{e^-} = 0\%$ , and  $\Lambda_{FF} = \infty$  are presented in Fig. 2 to observe a region that is sensitive to the aQGC. As can be seen from this figure, above  $p_T^\gamma > 300 \text{ GeV}$ , it is understood that the signal begins the separation from

backgrounds ( $p_T^\gamma > 300$  GeV with tagged Cut-5). Since the other polarization options have the same behaviors, they will not be given separately here.

Therefore, Table II shows a summary of the kinematic cuts that we used in this work. The numbers of events after the flow of cuts in Table II are given in Tables III-V to represent the effects of the cuts used in the analysis of the signal and the relevant backgrounds for three different polarized electron beams ( $f_{T,1}/\Lambda^4 = f_{T,7}/\Lambda^4 = f_{T,9}/\Lambda^4 = 1$  TeV $^{-4}$  and  $\mathcal{L} = 500$  fb $^{-1}$  selected for illustrative aim). As can be seen in these tables that  $\tau\tau\gamma\gamma$  and  $\gamma\gamma\ell\ell$  backgrounds are reduced more than the SM background and the signal. Also, the number of expected events of the  $e^+e^- \rightarrow Z\gamma\gamma$  signal is a factor of 2-18 greater than the corresponding ones for the SM and the relevant background.

The first observable that we study is the total cross-sections for the process  $e^+e^- \rightarrow Z\gamma\gamma \rightarrow l^+l^-\gamma\gamma$  as a function of the anomalous  $f_{Tj}/\Lambda^4$  couplings, which are shown in Figs.3-11. Here, we consider unpolarized and polarized beams of electrons, that is  $P_{e^-} = -80\%, 0\%, 80\%$  and three different values of the energy scale of the form factor,  $\Lambda_{FF} = 0.5, 1$  TeV and  $\infty$ . Also, each operator coefficient is scanned independently with all other operators set to zero. The results demonstrate a clear dependence of the cross section of the process  $e^+e^- \rightarrow Z\gamma\gamma \rightarrow l^+l^-\gamma\gamma$  with respect to the aQGC. As can be understood from these figures, the sensitivity of the aQGC  $f_{T,8}/\Lambda^4$  and  $f_{T,9}/\Lambda^4$  is more important than the other aQGC. Thus, we anticipate obtaining better limits on the  $f_{T,8}/\Lambda^4$  and  $f_{T,1}/\Lambda^4$  couplings via the process  $e^+e^- \rightarrow Z\gamma\gamma \rightarrow l^+l^-\gamma\gamma$  at the CLIC.

In Refs. [6–8], the ATLAS and CMS Collaborations at the LHC report evidence on the production  $pp \rightarrow Z\gamma\gamma$ , which is accessible for the first time with 8 TeV and 20.3 fb $^{-1}$  data set and more recently with  $\sqrt{s} = 13$  TeV and  $\mathcal{L} = 137$  fb $^{-1}$ . In these papers, the measured cross-section is used to set limits on aQGC  $Z\gamma\gamma\gamma$  and  $ZZ\gamma\gamma$ . Its bounds on the aQGC  $Z\gamma\gamma\gamma$  and  $ZZ\gamma\gamma$  are obtained from a selection of the most relevant systematic uncertainties, which are of the order of 1 – 10%. The dominant systematic uncertainties come from the estimation of the backgrounds 9%, the systematic uncertainty coming from the jet-photon misidentification 5 – 6%, integrated luminosity 1 – 3%, photon efficiencies 3 – 6%. For more details, see Tables 4 and 1 from these references. Based on the systematic uncertainties reported in Refs.[6–8], and in order to obtain the sensitivity on the anomalous  $Z\gamma\gamma\gamma$  and  $ZZ\gamma\gamma$  couplings, we choose the systematic uncertainties of  $\delta_{sys} = 0\%, 5\%,$  and 10%, respectively.

TABLE III: Number of expected events for the process  $e^+e^- \rightarrow Z\gamma\gamma$ , SM and relevant backgrounds processes after applied cuts given in Table II.

Polarized beams, $P_{e^-} = -80\%$				
Kinematic cuts	Signal ( $f_{T1}/\Lambda^4 = 10 \text{ TeV}^{-4}$ )	SM	$e^-e^+ \rightarrow \tau\tau\gamma\gamma$	$e^-e^+ \rightarrow \gamma\gamma\ell\ell$
Cut-0	395	86	125	77
Cut-1	395	86	0	77
Cut-2	395	86	0	77
Cut-3	395	86	0	77
Cut-4	367	80	0	5
Cut-5	279	27	0	0
	Signal( $f_{T7}/\Lambda^4 = 1 \text{ TeV}^{-4}$ )	SM	$e^-e^+ \rightarrow \tau\tau\gamma\gamma$	$e^-e^+ \rightarrow \gamma\gamma\ell\ell$
Cut-0	196	86	125	77
Cut-1	196	86	0	77
Cut-2	196	86	0	77
Cut-3	196	86	0	77
Cut-4	182	80	0	5
Cut-5	119	27	0	0
	Signal( $f_{T9}/\Lambda^4 = 1 \text{ TeV}^{-4}$ )	SM	$e^-e^+ \rightarrow \tau\tau\gamma\gamma$	$e^-e^+ \rightarrow \gamma\gamma\ell\ell$
Cut-0	1600	86	125	77
Cut-1	1600	86	0	77
Cut-2	1600	86	0	77
Cut-3	1600	86	0	77
Cut-4	1490	80	0	5
Cut-5	968	27	0	0

### B. Expected sensitivity on the anomalous $\frac{f_{T,j}}{\Lambda^4}$ couplings at the CLIC

One-dimensional expected sensitivity on aQGC  $f_{T,j}/\Lambda^4$  at 95% C.L. are examined after Cut-5 given in Table II, as well as and  $\mathcal{L} = 1 \text{ ab}^{-1}$  ( $P_{e^-} = 80\%$ ),  $\mathcal{L} = 4 \text{ ab}^{-1}$  ( $P_{e^-} = -80\%$ ) and  $\mathcal{L} = 5 \text{ ab}^{-1}$  ( $P_{e^-} = 0\%$ ) considering systematic errors of  $\delta_{sys} = 0\%, 5\%$  and  $10\%$  at the

TABLE IV: Number of expected events for the process  $e^+e^- \rightarrow Z\gamma\gamma$ , SM and relevant backgrounds processes after applied cuts given in Table II.

Polarized beams, $P_{e^-} = 0\%$				
Kinematic cuts	Signal ( $f_{T1}/\Lambda^4 = 10 \text{ TeV}^{-4}$ )	SM	$e^-e^+ \rightarrow \tau\tau\gamma\gamma$	$e^-e^+ \rightarrow \gamma\gamma\ell\ell$
Cut-0	249	80	118	72
Cut-1	249	80	0	72
Cut-2	249	80	0	72
Cut-3	249	80	0	72
Cut-4	231	75	0	5
Cut-5	165	25	0	0
	Signal( $f_{T7}/\Lambda^4 = 1 \text{ TeV}^{-4}$ )	SM	$e^-e^+ \rightarrow \tau\tau\gamma\gamma$	$e^-e^+ \rightarrow \gamma\gamma\ell\ell$
Cut-0	170	80	118	72
Cut-1	170	80	0	72
Cut-2	170	80	0	72
Cut-3	170	80	0	72
Cut-4	158	75	0	5
Cut-5	101	25	0	0
	Signal( $f_{T9}/\Lambda^4 = 1 \text{ TeV}^{-4}$ )	SM	$e^-e^+ \rightarrow \tau\tau\gamma\gamma$	$e^-e^+ \rightarrow \gamma\gamma\ell\ell$
Cut-0	3130	80	118	72
Cut-1	3130	80	0	72
Cut-2	3130	80	0	72
Cut-3	3130	80	0	72
Cut-4	2902	75	0	5
Cut-5	2540	25	0	0

CLIC with center-of-mass energy of  $\sqrt{s} = 3 \text{ TeV}$ .

To investigate the sensitivity to the anomalous  $f_{T,j}/\Lambda^4$  couplings we use the chi-squared distribution:

TABLE V: Number of expected events for the process  $e^+e^- \rightarrow Z\gamma\gamma$ , SM and relevant backgrounds processes after applied cuts given in Table II.

Polarized beams, $P_{e^-} = 80\%$				
Kinematic cuts	Signal ( $f_{T1}/\Lambda^4 = 10 \text{ TeV}^{-4}$ )	SM	$e^-e^+ \rightarrow \tau\tau\gamma\gamma$	$e^-e^+ \rightarrow \gamma\gamma\ell\ell$
Cut-0	105	70	110	62
Cut-1	105	70	0	62
Cut-2	105	70	0	62
Cut-3	105	70	0	62
Cut-4	98	65	0	3
Cut-5	50	21	0	0
	Signal( $f_{T7}/\Lambda^4 = 1 \text{ TeV}^{-4}$ )	SM	$e^-e^+ \rightarrow \tau\tau\gamma\gamma$	$e^-e^+ \rightarrow \gamma\gamma\ell\ell$
Cut-0	145	70	110	62
Cut-1	145	70	0	62
Cut-2	145	70	0	62
Cut-3	145	70	0	62
Cut-4	135	65	0	3
Cut-5	85	21	0	0
	Signal( $f_{T9}/\Lambda^4 = 1 \text{ TeV}^{-4}$ )	SM	$e^-e^+ \rightarrow \tau\tau\gamma\gamma$	$e^-e^+ \rightarrow \gamma\gamma\ell\ell$
Cut-0	4700	70	110	62
Cut-1	4700	70	0	62
Cut-2	4700	70	0	62
Cut-3	4700	70	0	62
Cut-4	4358	65	0	3
Cut-5	3855	21	0	0

$$\chi^2(f_{T,j}/\Lambda^4) = \left( \frac{\sigma_{SM}(\sqrt{s}) - \sigma_{BSM}(\sqrt{s}, f_{T,j}/\Lambda^4)}{\sigma_{SM}(\sqrt{s})\sqrt{(\delta_{st})^2 + (\delta_{sys})^2}} \right)^2, \quad (23)$$

where  $\sigma_{SM}(\sqrt{s})$  is the cross-section in the SM and  $\sigma_{BSM}(\sqrt{s}, f_{T,j}/\Lambda^4)$  is the cross-section in the presence of BSM interactions, and  $\delta_{st} = \frac{1}{\sqrt{N_{SM}}}$  is the statistical error and  $\delta_{sys}$  is

the systematic error. The number of events is given by  $N_{SM} = \mathcal{L} \times \sigma_{SM}$ , where  $\mathcal{L}$  is the integrated luminosity of the CLIC.

In Tables VI-VIII and Figs. 12-19, expected sensitivities at 95% C.L. on the aQGC  $ZZ\gamma\gamma$  and  $Z\gamma\gamma\gamma$  through the process  $e^+e^- \rightarrow Z\gamma\gamma$  in the case of two decay channels at the CLIC with  $P_{e^-} = -80\%, 0\%, 80\%$ ,  $\delta_{sys} = 0\%, 5\%, 10\%$  and  $\Lambda_{FF} = 0.5, 1$  TeV and  $\infty$  are represented. Here, any couplings are calculated while fixing the other couplings to zero. In our work, the best CLIC sensitivity limits on the aQGC might reach up to the order of magnitude  $O(10^1 - 10^{-2})$ , respectively. As can be seen from these tables and figures, the  $f_{T,8}/\Lambda^4$  and  $f_{T,9}/\Lambda^4$  couplings have the best sensitivities among the aQGC, as we expected. Our best limits on the aQGC improve much better than the current experimental limits.

We also examine the limits on the aQGC separately for three different cases: systematic error, polarization and the energy scale of the form factor. First, the limits on the aQGC with systematic errors of 5% and 10% are weaker regarding the limits obtained without systematic error is considered. For example, in Table VIII,  $f_{T,8}/\Lambda^4$  and  $f_{T,9}/\Lambda^4$  couplings have the best sensitivities between the aQGC,  $f_{T,8}/\Lambda^4$  without systematic error are approximately 1.1 and 1.3 times better than 5% and 10% systematic error limits, respectively.

We now examine the effect of three different  $P_{e^-} = 80\%, 0\%, 80\%$  polarizations on the aQGC. In Figs.12-19, for  $P_{e^-} = -80\%, 0\%, 80\%$ , comparison of the current observed limits with sensitivity on  $f_{T,j}/\Lambda^4$  couplings for expected luminosities of  $\mathcal{L} = 100, 500, 1000, 4000, 5000$   $fb^{-1}$ , center-of-mass energy of 3 TeV and  $\Lambda_{FF} = \infty$  at the CLIC are given. It can be understood from Figs. 12-19 that while our best sensitivities on  $f_{T,0}/\Lambda^4$ ,  $f_{T,1}/\Lambda^4$ ,  $f_{T,2}/\Lambda^4$ ,  $f_{T,5}/\Lambda^4$  and  $f_{T,7}/\Lambda^4$  couplings at  $P_{e^-} = -80\%$  are more restrictive than the limits obtained for the other polarizations  $P_{e^-} = 0\%$  and  $80\%$ ,  $f_{T,6}/\Lambda^4$ ,  $f_{T,8}/\Lambda^4$  and  $f_{T,9}/\Lambda^4$  couplings determined at  $P_{e^-} = 0\%$  are more better than the sensitivities derived on the aQGC for the other polarizations. This is because the  $O_T$  operators examined in this study have different multi-boson topologies.

Finally, when we examine the energy scale of the form factor in Eq. 20, it is easy to understand that as the value of the energy scale increases, the sensitivities obtained on all aQGCs gradually improve, as can be seen from Tables VI-VIII and Figs. 12-19.

TABLE VI: Expected sensitivity at 95% C.L. on the aQGC  $ZZ\gamma\gamma$  and  $Z\gamma\gamma\gamma$  through the process  $e^+e^- \rightarrow Z\gamma\gamma$  in the case of two decay channels at the CLIC with  $P_{e^-} = 0\%, -80\%, 80\%$ ,  $\delta_{sys} = 0\%, 5\%, 10\%$  and  $\Lambda_{FF} = 0.5$  TeV are represented. Here, any couplings are calculated while fixing the other couplings to zero.

$\Lambda_{FF} = 500$ GeV				
$P_{e^-}$		0%	-80%	80%
Couplings (TeV <sup>-4</sup> )		$\mathcal{L} = 5 \text{ ab}^{-1}$	$\mathcal{L} = 4 \text{ ab}^{-1}$	$\mathcal{L} = 1 \text{ ab}^{-1}$
$f_{T0}/\Lambda^4$	$\delta = 0\%$	[-4.61; 4.41]	[-3.99; 3.32]	$[-1.53; 1.40] \times 10^1$
	$\delta = 5\%$	[-5.07; 4.87]	[-4.33; 3.65]	$[-1.56; 1.43] \times 10^1$
	$\delta = 10\%$	[-5.99; 5.79]	[-5.02; 4.34]	$[-1.64; 1.51] \times 10^1$
$f_{T1}/\Lambda^4$	$\delta = 0\%$	[-4.60; 4.40]	[-3.98; 3.31]	$[-1.52; 1.39] \times 10^1$
	$\delta = 5\%$	[-5.06; 4.86]	[-4.32; 3.64]	$[-1.55; 1.42] \times 10^1$
	$\delta = 10\%$	[-5.98; 5.78]	[-5.01; 4.33]	$[-1.63; 1.50] \times 10^1$
$f_{T2}/\Lambda^4$	$\delta = 0\%$	[-8.89; 9.69]	[-6.41; 8.72]	$[-2.83; 3.20] \times 10^1$
	$\delta = 5\%$	$[-0.99; 1.06] \times 10^1$	$[-0.71; 0.94] \times 10^1$	$[-2.89; 3.26] \times 10^1$
	$\delta = 10\%$	$[-1.17; 1.25] \times 10^1$	$[-0.85; 1.08] \times 10^1$	$[-3.06; 3.42] \times 10^1$
$f_{T5}/\Lambda^4$	$\delta = 0\%$	[-2.41; 2.10]	[-4.84; 4.81]	[-2.55; 2.38]
	$\delta = 5\%$	[-2.65; 2.33]	[-5.28; 5.25]	[-2.60; 2.43]
	$\delta = 10\%$	[-3.10; 2.79]	[-6.18; 6.15]	[-2.74; 2.57]
$f_{T6}/\Lambda^4$	$\delta = 0\%$	[-2.74; 2.75]	[-2.16; 2.76]	[-5.27; 5.82]
	$\delta = 5\%$	[-3.01; 3.03]	[-2.38; 2.98]	[-5.38; 5.93]
	$\delta = 10\%$	[-3.57; 3.59]	[-2.83; 3.44]	[-5.69; 6.24]
$f_{T7}/\Lambda^4$	$\delta = 0\%$	[-5.94; 5.63]	[-7.70; 7.17]	$[-0.79; 0.70] \times 10^1$
	$\delta = 5\%$	[-6.53; 6.22]	[-8.38; 7.85]	[-8.07; 7.11]
	$\delta = 10\%$	[-7.70; 7.39]	[-9.76; 9.23]	[-8.47; 7.52]
$f_{T8}/\Lambda^4$	$\delta = 0\%$	$[-4.94; 5.13] \times 10^{-1}$	$[-7.18; 7.84] \times 10^{-1}$	$[-6.03; 6.01] \times 10^{-1}$
	$\delta = 5\%$	$[-5.45; 5.64] \times 10^{-1}$	$[-7.86; 8.52] \times 10^{-1}$	$[-6.16; 6.14] \times 10^{-1}$
	$\delta = 10\%$	$[-6.47; 6.66] \times 10^{-1}$	$[-9.26; 9.92] \times 10^{-1}$	$[-6.49; 6.47] \times 10^{-1}$
$f_{T9}/\Lambda^4$	$\delta = 0\%$	[-1.06; 1.01]	[-1.75; 1.40]	[-1.44; 1.07]
	$\delta = 5\%$	[-1.17; 1.12]	[-1.89; 1.54]	[-1.47; 1.10]
	$\delta = 10\%$	[-1.38; 1.33]	[-2.18; 1.83]	[-1.54; 1.17]

TABLE VII: Same as Table VI, but for  $\Lambda_{FF} = 1 \text{ TeV}$ 

$\Lambda_{FF} = 1000 \text{ GeV}$				
$P_{e^-}$		0%	-80%	80%
Couplings ( $\text{TeV}^{-4}$ )		$\mathcal{L} = 5 \text{ ab}^{-1}$	$\mathcal{L} = 4 \text{ ab}^{-1}$	$\mathcal{L} = 1 \text{ ab}^{-1}$
$f_{T0}/\Lambda^4$	$\delta = 0\%$	$[-1.54; 1.44]$	$[-1.27; 1.14]$	$[-5.15; 4.59]$
	$\delta = 5\%$	$[-1.70; 1.59]$	$[-1.38; 1.25]$	$[-5.25; 4.69]$
	$\delta = 10\%$	$[-1.99; 1.89]$	$[-1.61; 1.48]$	$[-5.52; 4.96]$
$f_{T1}/\Lambda^4$	$\delta = 0\%$	$[-1.53; 1.43]$	$[-1.26; 1.13]$	$[-5.14; 4.58]$
	$\delta = 5\%$	$[-1.69; 1.58]$	$[-1.37; 1.24]$	$[-5.24; 4.68]$
	$\delta = 10\%$	$[-1.98; 1.88]$	$[-1.60; 1.47]$	$[-5.51; 4.95]$
$f_{T2}/\Lambda^4$	$\delta = 0\%$	$[-0.24; 0.39] \times 10^1$	$[-0.19; 0.32] \times 10^1$	$[-0.81; 1.22] \times 10^1$
	$\delta = 5\%$	$[-2.70; 4.18]$	$[-2.12; 3.41]$	$[-0.83; 1.24] \times 10^1$
	$\delta = 10\%$	$[-3.31; 4.79]$	$[-2.57; 3.86]$	$[-0.88; 1.29] \times 10^1$
$f_{T5}/\Lambda^4$	$\delta = 0\%$	$[-7.32; 7.27] \times 10^{-1}$	$[-1.25; 0.99]$	$[-8.65; 8.60] \times 10^{-1}$
	$\delta = 5\%$	$[-8.07; 8.01] \times 10^{-1}$	$[-1.36; 1.09]$	$[-8.83; 8.78] \times 10^{-1}$
	$\delta = 10\%$	$[-9.54; 9.49] \times 10^{-1}$	$[-1.56; 1.30]$	$[-9.31; 9.26] \times 10^{-1}$
$f_{T6}/\Lambda^4$	$\delta = 0\%$	$[-0.84; 0.96]$	$[-0.82; 0.90]$	$[-1.42; 1.77]$
	$\delta = 5\%$	$[-0.93; 1.05]$	$[-0.89; 0.97]$	$[-1.45; 1.80]$
	$\delta = 10\%$	$[-1.12; 1.23]$	$[-1.05; 1.13]$	$[-1.54; 1.89]$
$f_{T7}/\Lambda^4$	$\delta = 0\%$	$[-2.03; 1.79]$	$[-2.60; 2.11]$	$[-2.78; 2.29]$
	$\delta = 5\%$	$[-2.23; 1.98]$	$[-2.81; 2.31]$	$[-2.84; 2.34]$
	$\delta = 10\%$	$[-2.62; 2.37]$	$[-3.24; 2.76]$	$[-2.97; 2.48]$
$f_{T8}/\Lambda^4$	$\delta = 0\%$	$[-1.46; 1.92] \times 10^{-1}$	$[-2.29; 2.76] \times 10^{-1}$	$[-2.14; 1.86] \times 10^{-1}$
	$\delta = 5\%$	$[-1.63; 2.08] \times 10^{-1}$	$[-2.52; 2.99] \times 10^{-1}$	$[-2.18; 1.90] \times 10^{-1}$
	$\delta = 10\%$	$[-1.97; 2.42] \times 10^{-1}$	$[-2.99; 3.46] \times 10^{-1}$	$[-2.29; 2.02] \times 10^{-1}$
$f_{T9}/\Lambda^4$	$\delta = 0\%$	$[-3.49; 3.33] \times 10^{-1}$	$[-5.27; 4.98] \times 10^{-1}$	$[-0.48; 0.35]$
	$\delta = 5\%$	$[-3.83; 3.67] \times 10^{-1}$	$[-5.74; 5.45] \times 10^{-1}$	$[-4.85; 3.60] \times 10^{-1}$
	$\delta = 10\%$	$[-4.52; 4.36] \times 10^{-1}$	$[-6.70; 6.41] \times 10^{-1}$	$[-5.07; 3.82] \times 10^{-1}$

TABLE VIII: Same as Table VI, but for  $\Lambda_{FF} = \infty$  TeV

$\Lambda_{FF} = \infty$				
$P_{e^-}$		0%	-80%	80%
Couplings (TeV <sup>-4</sup> )		$\mathcal{L} = 5 \text{ ab}^{-1}$	$\mathcal{L} = 4 \text{ ab}^{-1}$	$\mathcal{L} = 1 \text{ ab}^{-1}$
$f_{T0}/\Lambda^4$	$\delta = 0\%$	$[-1.64; 1.59] \times 10^{-1}$	$[-1.33; 1.28] \times 10^{-1}$	$[-5.36; 5.13] \times 10^{-1}$
	$\delta = 5\%$	$[-1.80; 1.75] \times 10^{-1}$	$[-1.45; 1.40] \times 10^{-1}$	$[-5.49; 5.26] \times 10^{-1}$
	$\delta = 10\%$	$[-2.13; 2.08] \times 10^{-1}$	$[-1.69; 1.64] \times 10^{-1}$	$[-5.78; 5.55] \times 10^{-1}$
$f_{T1}/\Lambda^4$	$\delta = 0\%$	$[-1.63; 1.58] \times 10^{-1}$	$[-1.32; 1.27] \times 10^{-1}$	$[-5.35; 5.12] \times 10^{-1}$
	$\delta = 5\%$	$[-1.79; 1.74] \times 10^{-1}$	$[-1.44; 1.39] \times 10^{-1}$	$[-5.48; 5.25] \times 10^{-1}$
	$\delta = 10\%$	$[-2.12; 2.07] \times 10^{-1}$	$[-1.68; 1.63] \times 10^{-1}$	$[-5.77; 5.54] \times 10^{-1}$
$f_{T2}/\Lambda^4$	$\delta = 0\%$	$[-3.20; 3.31] \times 10^{-1}$	$[-2.59; 2.67] \times 10^{-1}$	$[-1.03; 1.09]$
	$\delta = 5\%$	$[-3.53; 3.64] \times 10^{-1}$	$[-2.83; 2.91] \times 10^{-1}$	$[-1.06; 1.11]$
	$\delta = 10\%$	$[-4.18; 4.29] \times 10^{-1}$	$[-3.32; 3.40] \times 10^{-1}$	$[-1.11; 1.17]$
$f_{T5}/\Lambda^4$	$\delta = 0\%$	$[-7.77; 7.23] \times 10^{-2}$	$[-7.62; 7.00] \times 10^{-2}$	$[-1.25; 1.23] \times 10^{-1}$
	$\delta = 5\%$	$[-8.53; 7.99] \times 10^{-2}$	$[-8.29; 7.66] \times 10^{-2}$	$[-1.27; 1.25] \times 10^{-1}$
	$\delta = 10\%$	$[-1.00; 0.95] \times 10^{-1}$	$[-9.65; 9.03] \times 10^{-2}$	$[-1.34; 1.32] \times 10^{-1}$
$f_{T6}/\Lambda^4$	$\delta = 0\%$	$[-9.48; 9.65] \times 10^{-2}$	$[-1.15; 1.24] \times 10^{-1}$	$[-1.11; 1.40] \times 10^{-1}$
	$\delta = 5\%$	$[-1.05; 1.06] \times 10^{-1}$	$[-1.26; 1.35] \times 10^{-1}$	$[-1.14; 1.43] \times 10^{-1}$
	$\delta = 10\%$	$[-1.24; 1.26] \times 10^{-1}$	$[-1.48; 1.57] \times 10^{-1}$	$[-1.20; 1.50] \times 10^{-1}$
$f_{T7}/\Lambda^4$	$\delta = 0\%$	$[-2.22; 1.92] \times 10^{-1}$	$[-2.39; 2.15] \times 10^{-1}$	$[-3.06; 2.88] \times 10^{-1}$
	$\delta = 5\%$	$[-2.43; 2.13] \times 10^{-1}$	$[-2.59; 2.35] \times 10^{-1}$	$[-3.04; 3.02] \times 10^{-1}$
	$\delta = 10\%$	$[-2.85; 2.55] \times 10^{-1}$	$[-3.01; 2.77] \times 10^{-1}$	$[-3.21; 3.18] \times 10^{-1}$
$f_{T8}/\Lambda^4$	$\delta = 0\%$	$[-1.78; 1.85] \times 10^{-2}$	$[-2.44; 3.04] \times 10^{-2}$	$[-2.21; 2.13] \times 10^{-2}$
	$\delta = 5\%$	$[-1.96; 2.03] \times 10^{-2}$	$[-2.68; 3.29] \times 10^{-2}$	$[-2.26; 2.18] \times 10^{-2}$
	$\delta = 10\%$	$[-2.33; 2.40] \times 10^{-2}$	$[-3.19; 3.79] \times 10^{-2}$	$[-2.38; 2.30] \times 10^{-2}$
$f_{T9}/\Lambda^4$	$\delta = 0\%$	$[-3.83; 3.48] \times 10^{-2}$	$[-5.83; 5.17] \times 10^{-2}$	$[-4.39; 4.35] \times 10^{-2}$
	$\delta = 5\%$	$[-4.20; 3.85] \times 10^{-2}$	$[-6.32; 5.66] \times 10^{-2}$	$[-4.48; 4.44] \times 10^{-2}$
	$\delta = 10\%$	$[-4.94; 4.59] \times 10^{-2}$	$[-7.34; 6.69] \times 10^{-2}$	$[-4.72; 4.68] \times 10^{-2}$

## IV. RESULTS AND CONCLUSIONS

The Effective Field Theory framework represents a general way to parametrize new physics phenomena, which extends the SM by considering new interactions between its constituent particles. A specific class of these interactions is labeled as the aQGC. Investigating the aQGC described by the non-Abelian gauge symmetry within the framework of the SM may lead to an additional confirmation of the model and give clues to the existence of new physics. The LHC maybe provide discoveries and valuable information. On the other hand, it is usually agreed that the clean and precise environment of the linear colliders according to the LHC is ideally suited to the examination for new physics. In addition, the use of polarized beams plays a significant role in the physics programs of future linear colliders. In additional, since the aQGC defined through effective Lagrangian have dimension-8, they have strong energy dependence. Thus, the anomalous cross-section containing the anomalous  $ZZ\gamma\gamma$  and  $Z\gamma\gamma\gamma$  vertices has higher than the SM cross-section. Therefore, future linear colliders such as CLIC with high center-of-mass energy and luminosity could provide us with possible new physics signs beyond the SM. With these motivations, we perform a detailed study of the process  $e^-e^+ \rightarrow Z\gamma\gamma \rightarrow \ell^+\ell^-\gamma\gamma$  at the CLIC to probe the aQGC  $Z\gamma\gamma\gamma$  and  $ZZ\gamma\gamma$  in a model-independent way. Here, the  $\ell^+\ell^-\gamma\gamma$  production yield as a function of a kinematic variable particularly sensitive to the anomalous couplings is used. In order to determine optimum kinematic cuts that the signal dominates the relevant background, we perform the transverse momentums, pseudo-rapidities, angular  $\Delta R$  distributions for the leptons and photons in the final state of the process using cut-based techniques. Among the eight operators, we see that the  $O_{T,8}$  and  $O_{T,9}$  operators have the best sensitivities since they only contain the neutral electroweak gauge bosons.

In conclusion, we have shown that the study of the process  $e^+e^- \rightarrow Z\gamma\gamma \rightarrow \ell^+\ell^-\gamma\gamma$  at the CLIC can test aQGC  $f_{T,j}/\Lambda^4$  that are two orders of magnitude stronger than the existing limits from direct searches reported by the current experimental limits. In particular, stringent sensitivities are placed on the anomalous  $f_{T,8,9}/\Lambda^4$  couplings of:  $\frac{f_{T8}}{\Lambda^4} = [-1.78; 1.85] \times 10^{-2} \text{ TeV}^{-4}$ ,  $\frac{f_{T9}}{\Lambda^4} = [-3.83; 3.48] \times 10^{-2} \text{ TeV}^{-4}$ , with  $\sqrt{s} = 3 \text{ TeV}$ ,  $\mathcal{L} = 5 \text{ ab}^{-1}$ ,  $P_{e^-} = 0\%$ ,  $\delta_{sys} = 0\%$  and  $\Lambda_{FF} = \infty$ . Furthermore, if a signal is observed, the comparison of the process here studied, which is sensitive only to photonic quartic operators, with the observations for processes also dependent on nonphotonic couplings, such as weak gauge bo-

son pair production, could reveal some symmetries of the underlying dynamics. Therefore, if the experimental measurement of the aQGC were to be confirmed, then nature could have provided us with the technique and the signal appropriate to study the full spectroscopy of the aQGC.

### Acknowledgements

A. G. R. and M. A. H. R. thank SNI and PROFEXCE (México). The numerical calculations reported in this paper were fully performed at TUBITAK ULAKBIM, High Performance and Grid Computing Center (TRUBA resources).

- 
- [1] S. L. Glashow, *Nucl. Phys.* **22**, 579 (1961).
  - [2] S. Weinberg, *Phys. Rev. Lett.* **19**, 1264 (1967).
  - [3] A. Salam, in *Elementary Particle Theory*, Ed. N. Svartholm (Almqvist and Wiskell, Stockholm, 1968) 367.
  - [4] P. A. Zyla, *et al.*, [Particle Data Group], *Prog. Theor. Exp. Phys.* **2020**, 083C01 (2020).
  - [5] A. Tumasyan, *et al.*, [CMS Collaboration], [arXiv:2106.11082 [hep-ex]].
  - [6] G. Aad, *et al.*, [ATLAS Collaboration], *Phys. Rev. D* **93**, 112002 (2016).
  - [7] A. M. Sirunyan, *et al.*, [CMS Collaboration], *JHEP* **10**, 072 (2017).
  - [8] A. Tumasyan, *et al.*, [CMS Collaboration], *JHEP* **10**, 174 (2021).
  - [9] P. Achard, *et al.*, [L3 Collaboration], *Phys. Lett. B* **540**, 43-51 (2002).
  - [10] G. Abbiendi, *et al.*, [OPAL Collaboration], *Phys. Rev. D* **70**, 032005 (2004).
  - [11] B. Abbott, *et al.*, [D0 Collaboration], *Phys. Rev. D* **62**, 052005 (2000).
  - [12] V. M. Abazov, *et al.*, [D0 Collaboration], *Phys. Rev. D* **88**, 012005 (2013).
  - [13] G. Aad, *et al.*, [ATLAS Collaboration], *Phys. Rev. Lett.* **113**, 141803 (2014).
  - [14] G. Aad, *et al.*, [ATLAS Collaboration], *Phys. Rev. Lett.* **115**, 031802 (2015).
  - [15] M. Aaboud, *et al.*, [ATLAS Collaboration], *Phys. Rev. D* **96**, 012007 (2017).
  - [16] M. Aaboud, *et al.*, [ATLAS Collaboration], *Eur. Phys. J. C* **77**, 646 (2017).
  - [17] M. Aaboud, *et al.*, [ATLAS Collaboration], *Phys. Rev. D* **95**, 032001 (2017).
  - [18] S. Chatrchyan, *et al.*, [CMS Collaboration], *Phys. Rev. D* **90**, 032008 (2014).

- [19] A. M. Sirunyan, *et al.*, [CMS Collaboration], *Phys. Lett. B* **774**, 682 (2017).
- [20] V. Khachatryan, *et al.*, [CMS Collaboration], *Phys. Lett. B* **770**, 380 (2017).
- [21] V. Khachatryan, *et al.*, [CMS Collaboration], *JHEP* **06**, 106 (2017).
- [22] A. M. Sirunyan, *et al.*, [CMS Collaboration], *Phys. Rev. Lett.* **120**, 081801 (2018).
- [23] A. M. Sirunyan, *et al.*, [CMS Collaboration], *Phys. Lett. B* **795**, 281 (2019).
- [24] A. M. Sirunyan, *et al.*, [CMS Collaboration], *Phys. Lett. B* **798**, 134985 (2019).
- [25] A. M. Sirunyan, *et al.* [CMS Collaboration], *Phys. Lett. B* **812**, 135992 (2021).
- [26] A. M. Sirunyan, *et al.*, [CMS Collaboration], *JHEP* **06**, 076 (2020).
- [27] A. M. Sirunyan, *et al.*, [CMS Collaboration], *Phys. Lett. B* **809**, 135710 (2020).
- [28] A. M. Sirunyan, *et al.*, [CMS Collaboration], *Phys. Lett. B* **811**, 135988 (2020).
- [29] W. J. Stirling, A. Werthenbach, *Eur. Phys. J.* **C14**, 103 (2000).
- [30] A. Gutiérrez-Rodríguez, C. G. Honorato, J. Montano, and M. A. Pérez, *Phys. Rev.* **D89**, 034003 (2014).
- [31] G. Belanger, F. Boudjema, Y. Kurihara, D. Perret-Gallix, and A. Semenov, *Eur. Phys. J.* **C13**, 283 (2000).
- [32] G. Montagna, M. Moretti, O. Nicosini, M. Osmo, F. Piccinini, *Phys. Lett.* **B515**, 197 (2001).
- [33] O. J. P. Eboli, M. C. Gonzalez-Garcia and S. F. Novaes, *Nucl. Phys.* **B411**, 381 (1994).
- [34] S. Atag and I. Sahin, *Phys. Rev.* **D75**, 073003 (2007).
- [35] M. Koksál, VARI, A. Senol, *Adv. High Energy Phys.* **2016**, 8672391.
- [36] M. koksál, *Eur. Phys. J. Plus* **130**, 75 (2015).
- [37] P. J. Dervan, A. Signer, W. J. Stirling, and A. Werthenbach, *J. Phys.* **G26**, 607 (2000).
- [38] O. J. P. Eboli, M. C. Gonzalez-Garcia, and S. M. Lietti, S. F. Novaes, *Phys. Rev.* **D63**, 075008 (2001).
- [39] E. Chapon, C. Royon and O. Kepka, *Phys. Rev.* **D81**, 074003 (2010).
- [40] R. S. Gupta, *Phys. Rev.* **D85**, 014006 (2012).
- [41] J. de Favereau de Jeneret, V. Lemaitre, Y. Liu, S. Ovin, T. Pierzchala, K. Piotrkowski, X. Rouby, N. Schul, M. Vander Donckt, arXiv:0908.2020.
- [42] A. Senol, arXiv:1311.1370.
- [43] I. Sahin and B. Sahin, *Phys. Rev.* **D86**, 115001 (2012).
- [44] O. J. P. Eboli, M. C. Gonzalez-Garcia, and S. M. Lietti, *Phys. Rev.* **D69**, 095005 (2004).
- [45] A. Senol, C. O. Karadeniz, K. Y. Oyulmaz, C. Helveci, and H. Denizli, arXiv:2109.12572

[hep-ph].

- [46] R. Franceschini, P. Roloff, U. Schnoor and A. Wulzer, The Compact Linear Collider (CLIC): Physics Potential, arXiv: 1812.07986.
- [47] K. Fujii *et al.* [LCC Physics Working Group], DESY 17-237, KEK Preprint 2017-57, SLAC-PUB-17197
- [48] S. Dawson, C. Englert, and T. Plehn, arXiv:1808.01324 [hep-ph].
- [49] O. J. P. Eboli, M. C. Gonzalez-Garcia, and S. F. Novaes, *Nucl. Phys.* **B411**, 381 (1994).
- [50] O. J. P. Eboli, M. B. Magro, P. G. Mercadante, and S. F. Novaes, *Phys. Rev.* **D52**, 15 (1995).
- [51] O. J. P. Eboli, M. C. Gonzalez-Garcia, and S. M. Lietti, S. F. Novaes, *Phys. Rev.* **D63**, 075008 (2001).
- [52] O. J. P. Eboli, M. C. Gonzalez-Garcia, and S. M. Lietti, *Phys. Rev.* **D69**, 095005 (2004).
- [53] O. J. P. Eboli, M. C. Gonzalez-Garcia and J. K. Mizukoshi, *Phys. Rev.* **D74**, 073005 (2006).
- [54] E. da Silva Almeida, O. J. P. Éboli, M. C. Gonzalez-Garcia, *Phys. Rev.* **D101**.
- [55] C. Degrande, *et al.*, arXiv: 1309.7890.
- [56] J. Alwall, M. Herquet, F. Maltoni, O. Mattelaer and T. Stelzer, *JHEP* **06**, 128 (2011).
- [57] A. Alloul, N. D. Christensen, C. Degrande, C. Duhr and B. Fuks, *Comput. Phys. Commun.* **185**, 2250 (2014).
- [58] C. Degrande, C. Duhr, B. Fuks, D. Grellscheid, O. Mattelaer and T. Reiter, *Comput. Phys. Commun.* **183**, 1201 (2012).

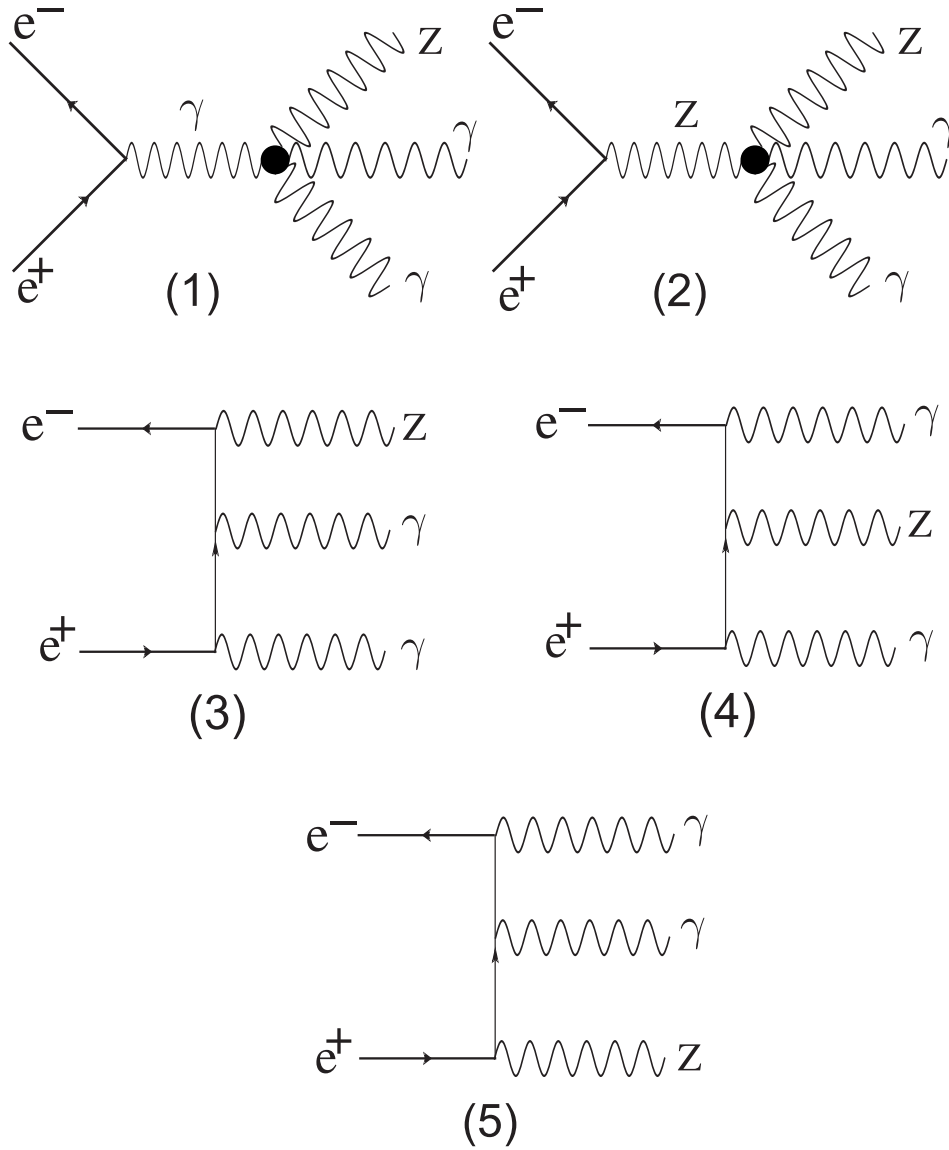


FIG. 1: Feynman diagrams for the signal process  $e^+e^- \rightarrow Z\gamma\gamma$  induced by the effective  $ZZ\gamma\gamma$  and  $Z\gamma\gamma\gamma$  vertices. New physics (represented by a black circle) in the electroweak sector can modify the aQGC.

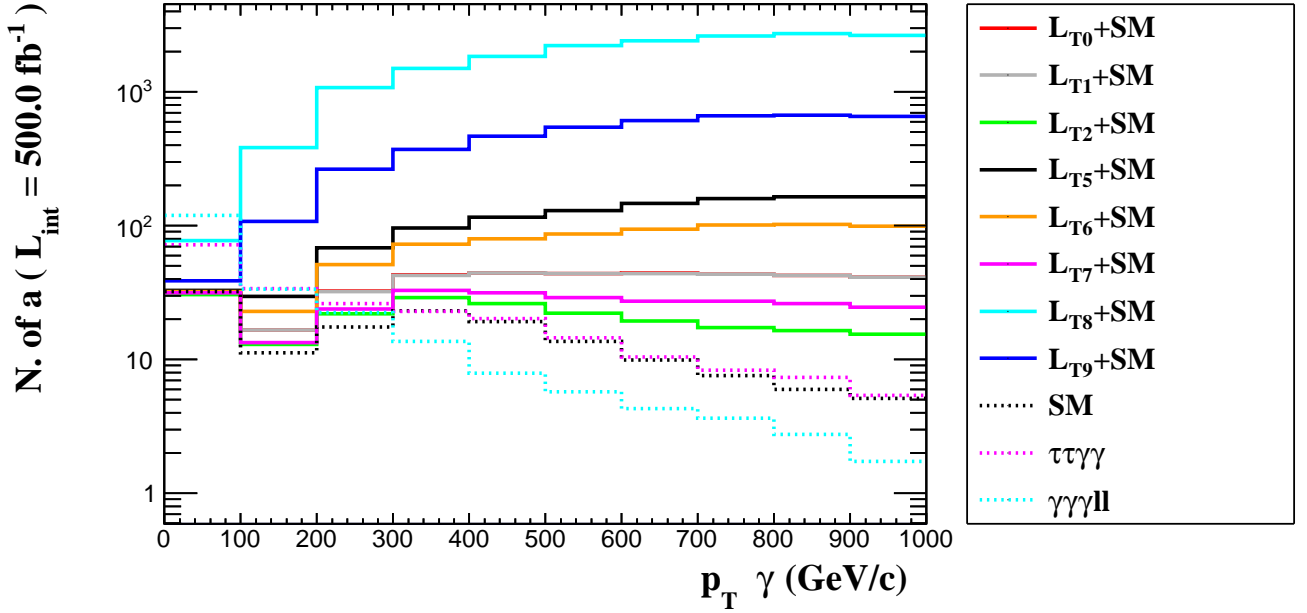


FIG. 2: The number of expected events as a function of  $p_T^\gamma$  photon transverse momentum for the  $e^+e^- \rightarrow Z\gamma\gamma$  signal and backgrounds at the CLIC with  $\sqrt{s} = 3$  TeV,  $P_{e^-} = 0\%$ , and  $\Lambda_{FF} = \infty$ . The distributions are for  $f_{T,j}/\Lambda^4$  with  $i = 0, 1, 2, 5, 6, 7, 8, 9$  and relevant backgrounds.

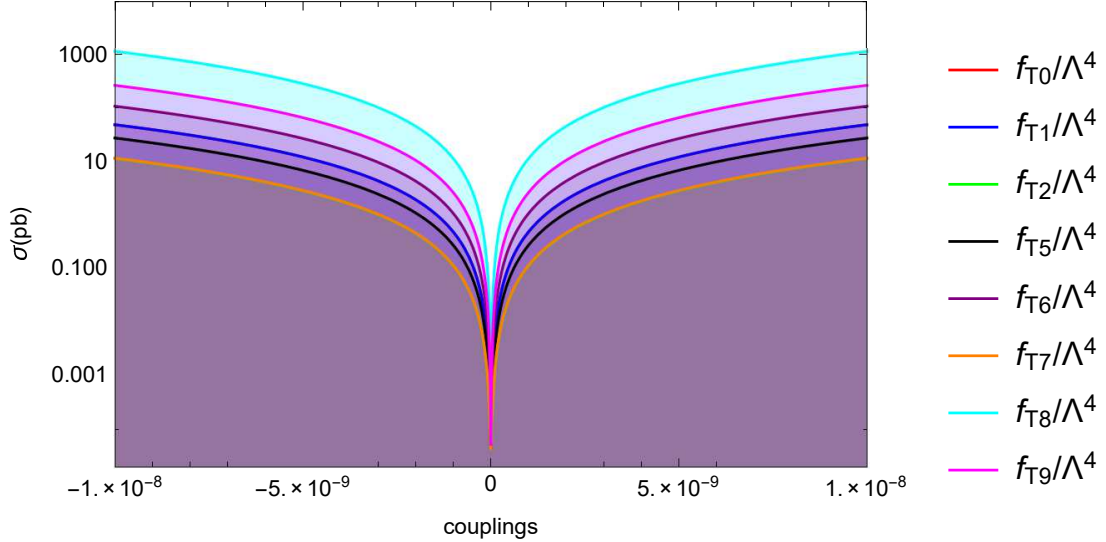


FIG. 3: Production cross-section for the process  $e^+e^- \rightarrow Z\gamma\gamma$  in terms of the aQGC  $f_{T,j}/\Lambda^4$  for the CLIC with  $\sqrt{s} = 3$  TeV,  $\Lambda_{FF} = 0.5$  TeV and polarized beams  $P_{e^-} = -80\%$ .

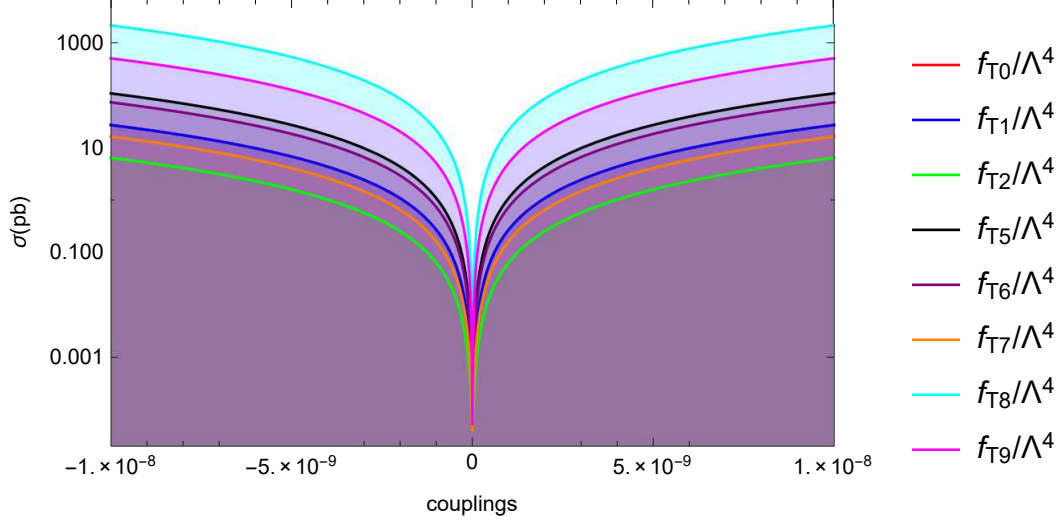


FIG. 4: Same as in Fig. 3, but for  $P_{e^-} = 0\%$ .

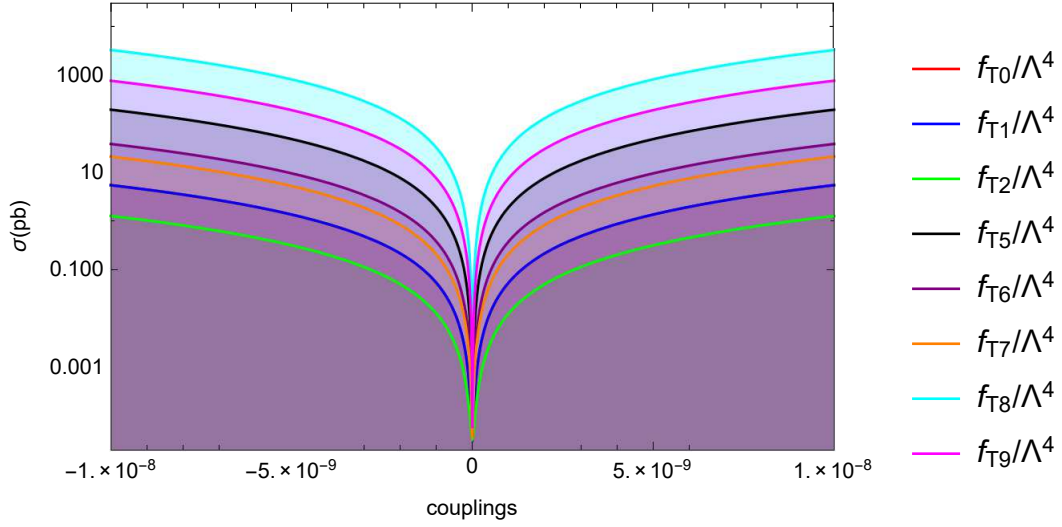


FIG. 5: Same as in Fig. 3, but for  $P_{e^-} = 80\%$ .

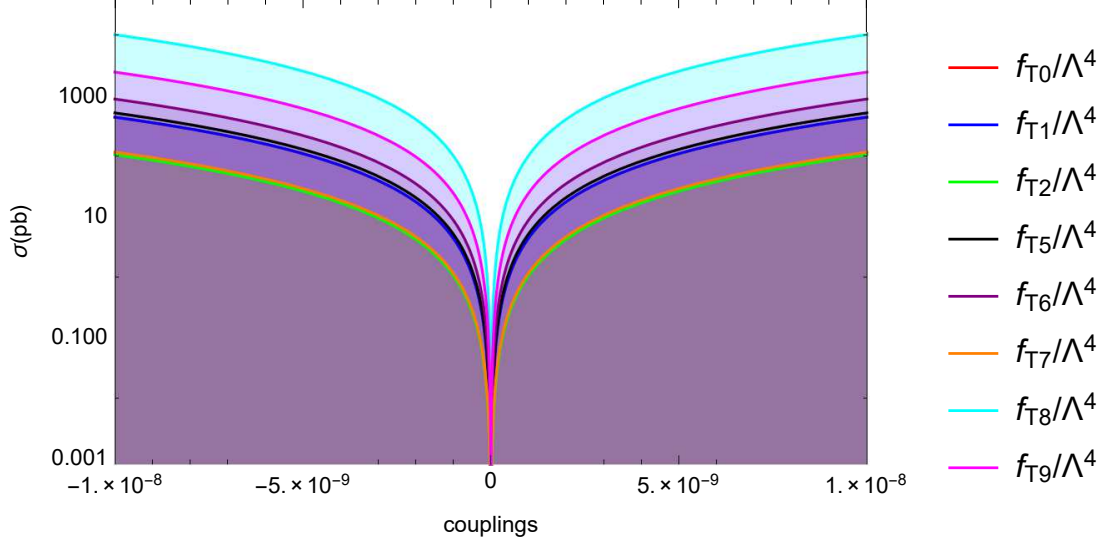


FIG. 6: Production cross-section for the process  $e^+e^- \rightarrow Z\gamma\gamma$  signal in terms of the aQGC  $f_{T,j}/\Lambda^4$  for the CLIC with  $\sqrt{s} = 3$  TeV,  $\Lambda_{FF} = 1$  TeV and polarized beams  $P_{e^-} = -80\%$ .

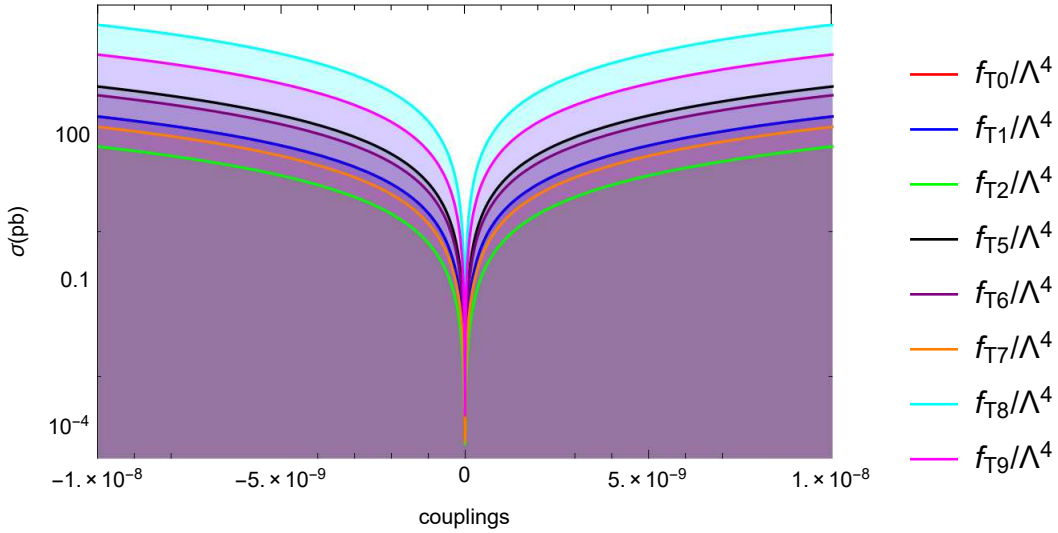


FIG. 7: Same as in Fig. 6, but for  $P_{e^-} = 0\%$ .

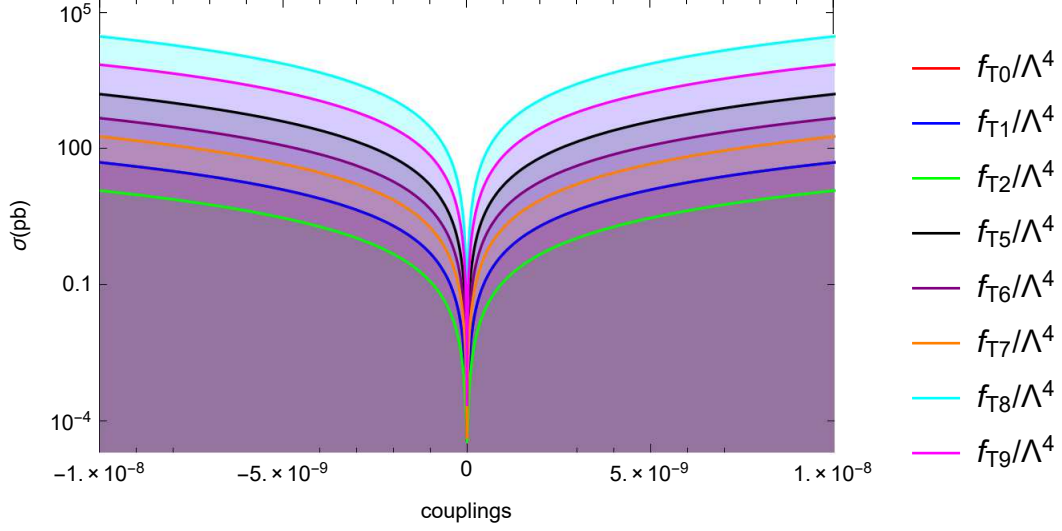


FIG. 8: Same as in Fig. 6, but for  $P_{e^-} = 80\%$ .

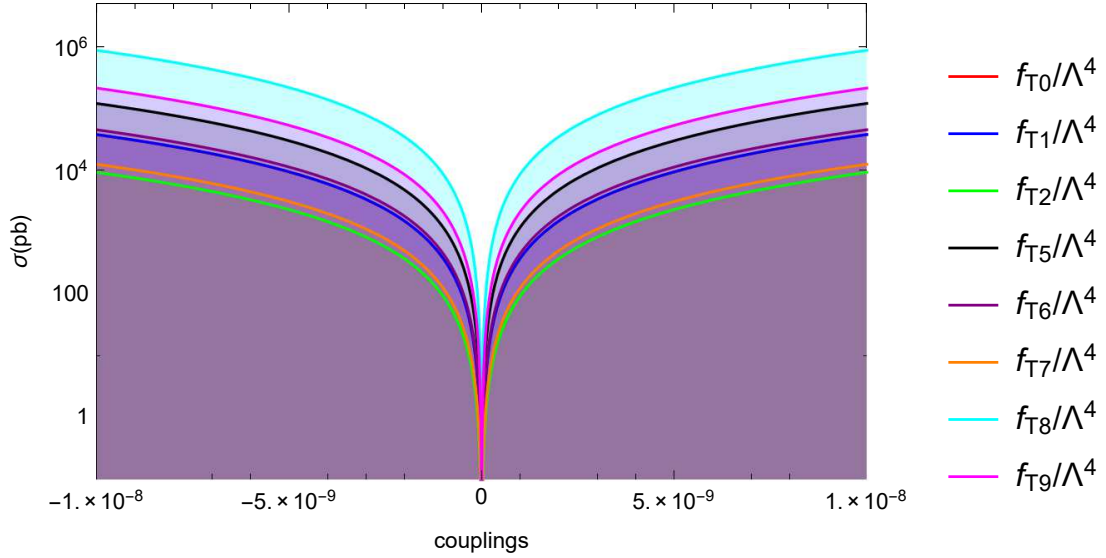


FIG. 9: Production cross-section for the process  $e^+e^- \rightarrow Z\gamma\gamma$  in terms of the aQGC  $f_{T,j}/\Lambda^4$  for the CLIC with  $\sqrt{s} = 3$  TeV,  $\Lambda_{FF} = \infty$  and polarized beams  $P_{e^-} = -80\%$ .

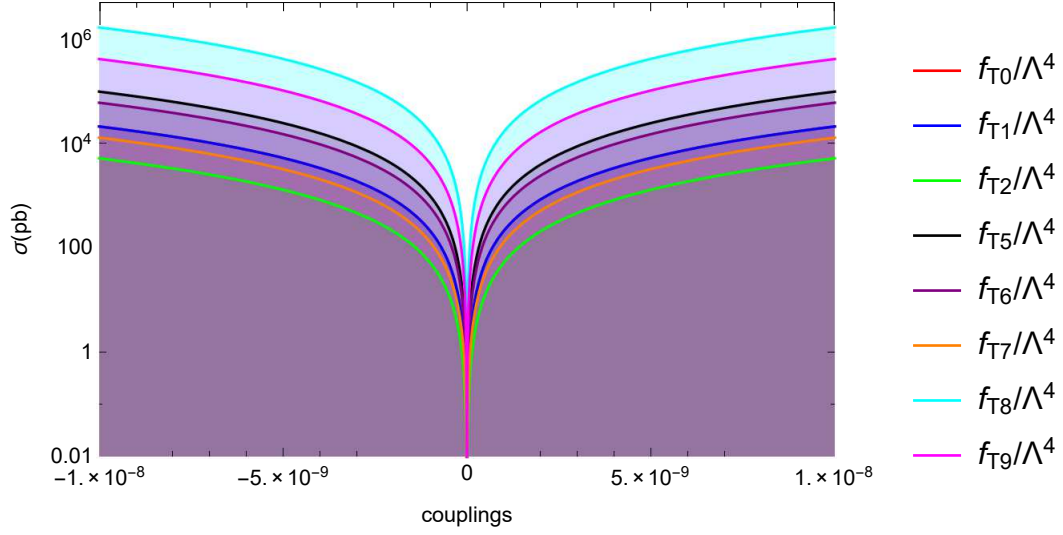


FIG. 10: Same as in Fig. 9, but for  $P_{e^-} = 0\%$ .

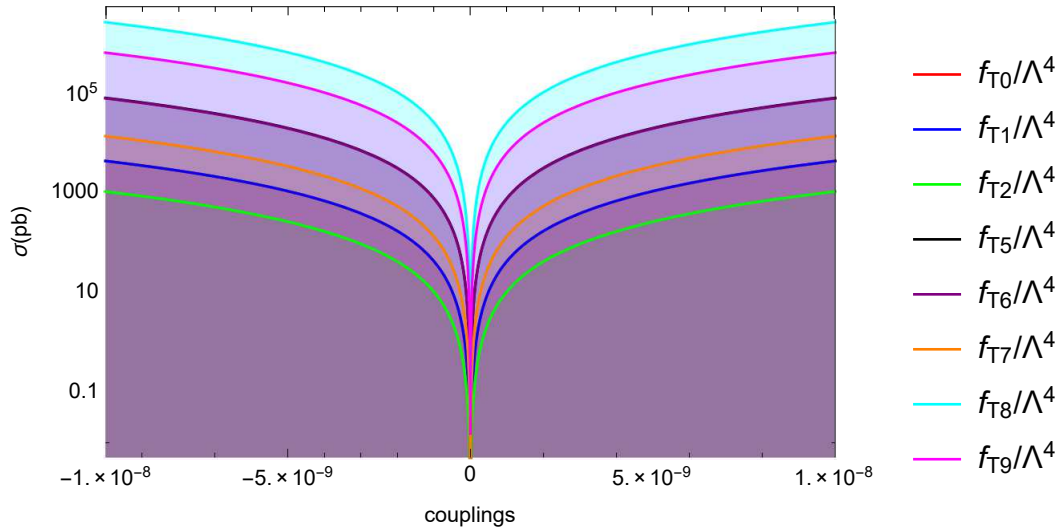


FIG. 11: Same as in Fig. 9, but for  $P_{e^-} = 80\%$ .

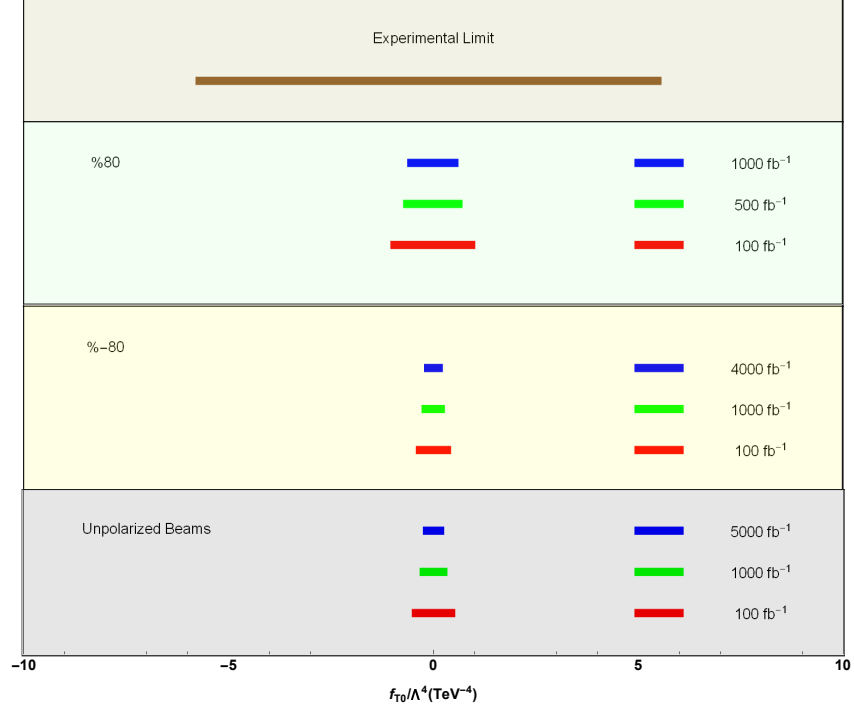


FIG. 12: Comparison of the current experimental limits and projected sensitivity on  $f_{T,0}/\Lambda^4$  for expected luminosities of  $\mathcal{L} = 100, 500, 1000, 4000, 5000 \text{ fb}^{-1}$  and  $\sqrt{s} = 3 \text{ TeV}$  at the CLIC. We consider  $P_{e^-} = -80\%, 0\%, 80\%$ .

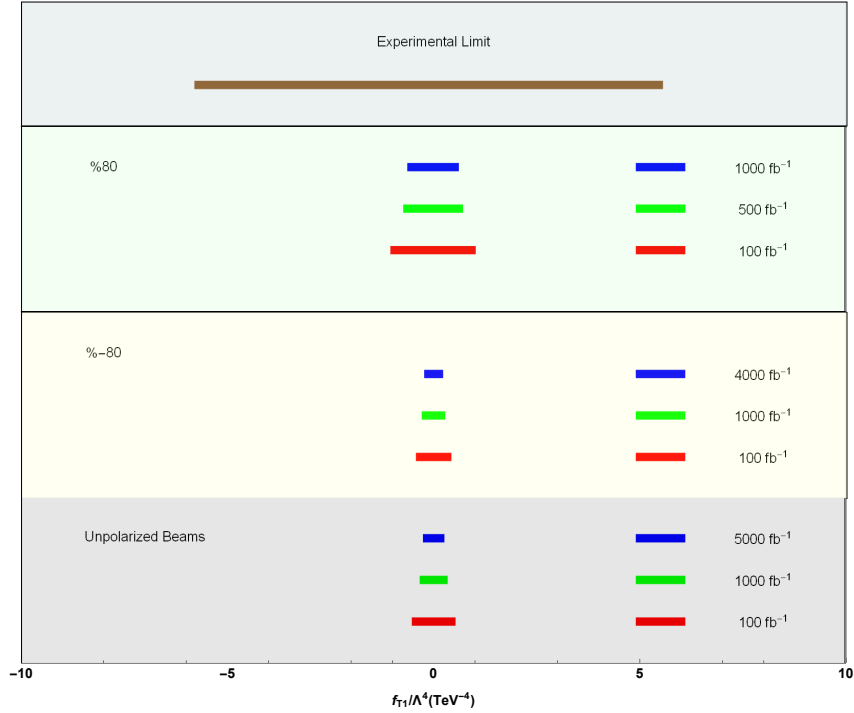


FIG. 13: Same as in Fig. 12, but for  $f_{T,1}/\Lambda^4$ .

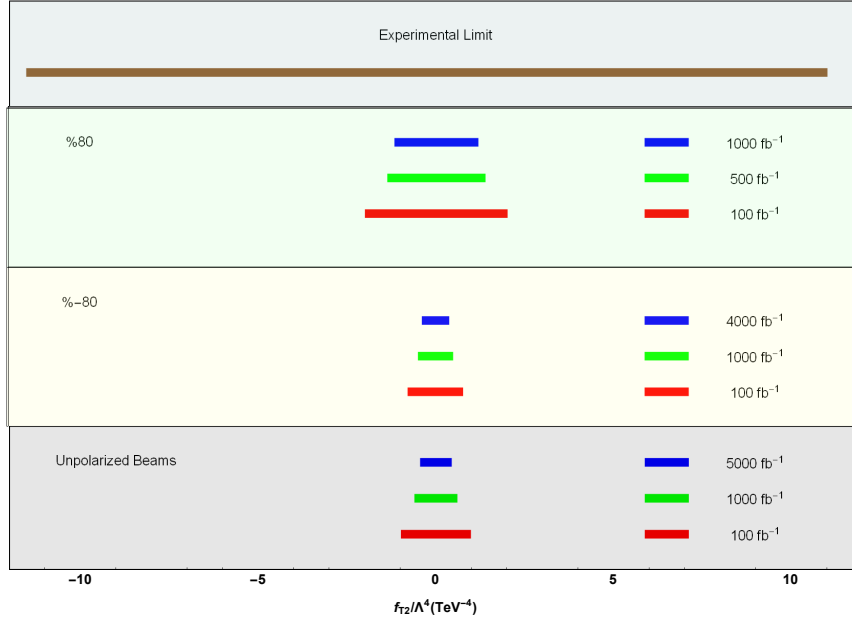


FIG. 14: Same as in Fig. 12, but for  $f_{T,2}/\Lambda^4$ .

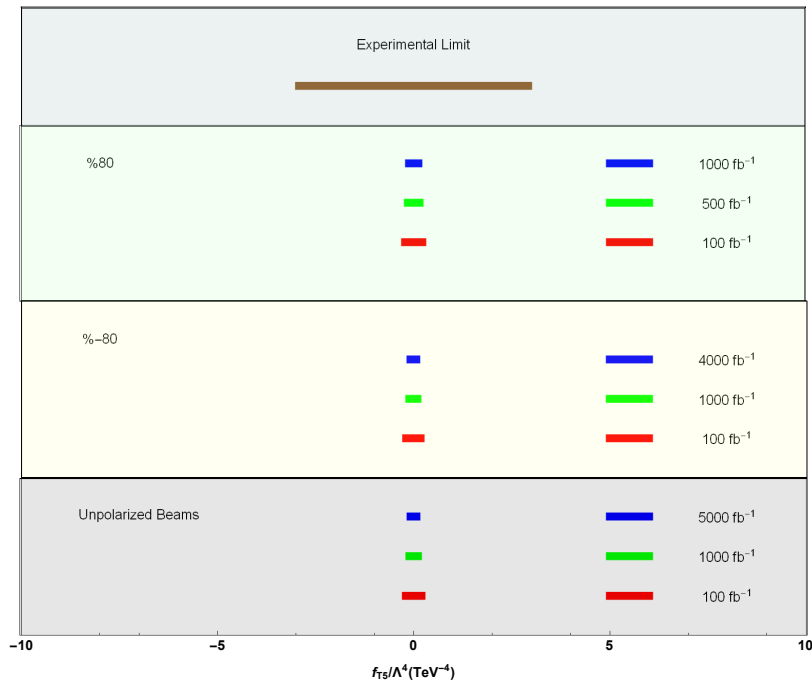


FIG. 15: Same as in Fig. 12, but for  $f_{T,5}/\Lambda^4$ .

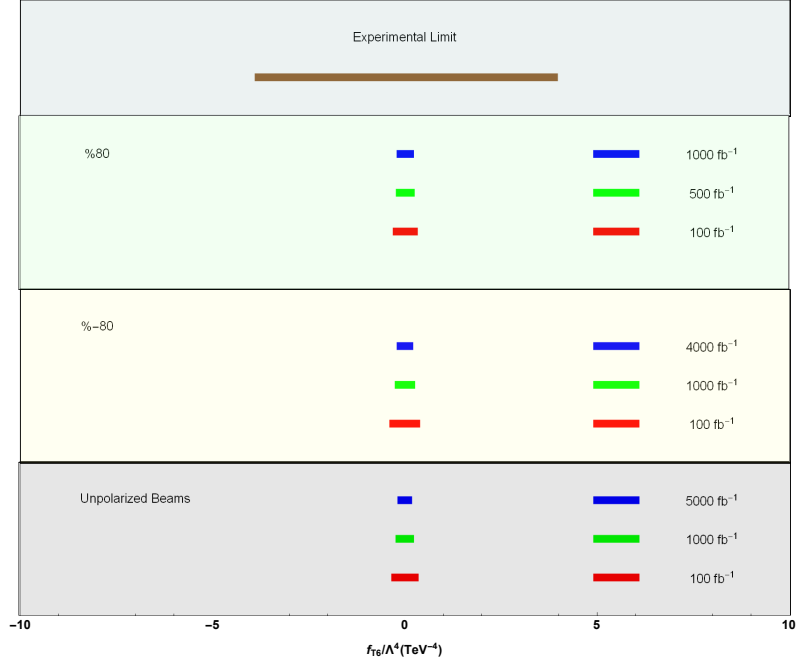


FIG. 16: Same as in Fig. 12, but for  $f_{T,6}/\Lambda^4$ .

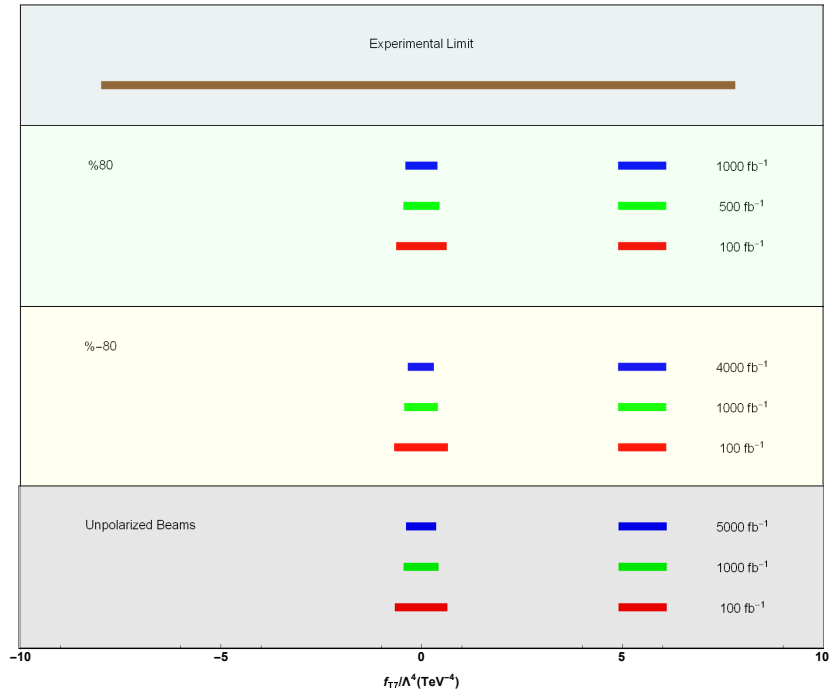


FIG. 17: Same as in Fig. 12, but for  $f_{T,7}/\Lambda^4$ .

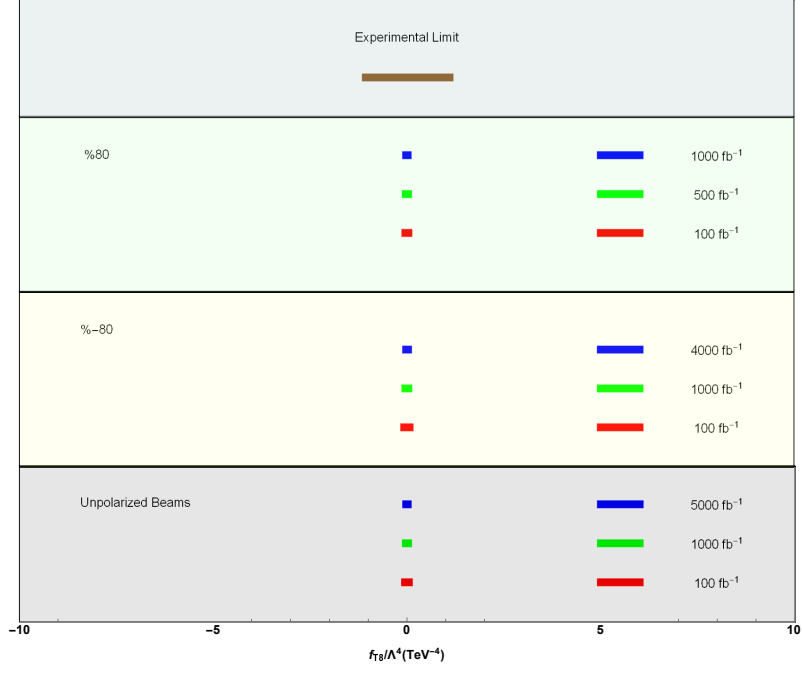


FIG. 18: Same as in Fig. 12, but for  $f_{T,8}/\Lambda^4$ .

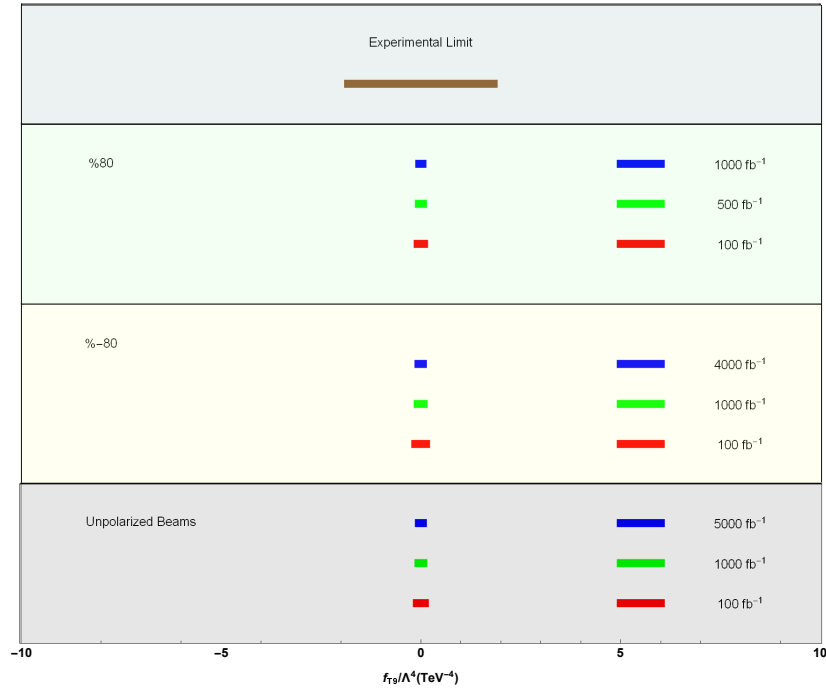


FIG. 19: Same as in Fig. 12, but for  $f_{T,9}/\Lambda^4$ .